Title

Membrane Protein Properties Revealed through Data-Rich Electrostatics Calculations

Journal

Structure, 23(8)

ISSN

1359-0278

Authors

Marcoline, Frank V

Bethel, Neville

Guerriero, Christopher J

et al.

Publication Date

2015-08-01

DOI

10.1016/j.str.2015.05.014

Peer reviewed

HHS Public Access

Author manuscript

Structure. Author manuscript; available in PMC 2016 August 04.

Published in final edited form as:

Structure. 2015 August 4; 23(8): 1526–1537. doi:10.1016/j.str.2015.05.014.

Membrane protein properties revealed through data-rich electrostatics calculations

Frank V. Marcoline[#1,2], **Neville Bethel**[#1,2,3], **Christopher J. Guerriero**[4], **Jeffrey L. Brodsky**[4], and **Michael Grabe**[1,2,*]

[1] Cardiovascular Research Institute, University of California, San Francisco, CA 94158, USA

[2] Department of Pharmaceutical Chemistry, University of California, San Francisco, CA 94158, USA

[3] Integrative Program in Quantitative Biology, University of California, San Francisco, CA 94158, USA

[4] Department of Biological Sciences, University of Pittsburgh, Pittsburgh, PA 15260, USA

[#] These authors contributed equally to this work.

SUMMARY

The electrostatic properties of membrane proteins often reveal many of their key biophysical characteristics, such as ion channel selectivity and the stability of charged membrane-spanning segments. The Poisson-Boltzmann (PB) equation is the gold standard for calculating protein electrostatics, and the software APBSmem enables the solution of the PB equation in the presence of a membrane. Here, we describe significant advances to APBSmem including: full automation of system setup, per-residue energy decomposition, incorporation of PDB2PQR, calculation of membrane induced pK_a shifts, calculation of non-polar energies, and command-line scripting for large scale calculations. We highlight these new features with calculations carried out on a number of membrane proteins, including the recently solved structure of the ion channel TRPV1 and a large survey of 1,614 membrane proteins of known structure. This survey provides a comprehensive list of residues with large electrostatic penalties for being embedded in the membrane potentially revealing interesting functional information.

[*]Correspondence: michael.grabe@ucsf.edu.

AUTHOR CONTRIBUTIONS

F.V.M., N.B. and M.G. designed all aspects of the research project, while C.J.G. and J.L.B. aided in the design of Case V. F.V.M. and N.B. programmed the new functionality into APBSmem code and carried out all calculations. All authors contributed to writing and editing the manuscript.

SUPPLEMENTAL INFORMATION

Supplemental Information includes 3 figures, detailed descriptions of new APBSmem features, derivations of electrostatic energies for Cases I-III, a full description of our pKa calculation methodology, details of the homology model construction of Ste6p* with Modeller9v13, and command line scripting for the heat map in Figure 8. The Supplemental Information for this article can be found online at doi:XXXX.

INTRODUCTION

The Poisson-Boltzmann (PB) equation is a popular method for calculating the electrostatic properties of proteins (Baker et al., 2001; Brooks et al., 2009; Gilson and Honig, 1987; Grant et al., 2001; Zhou et al., 2008). The equation relates the fixed charges on a protein of known structure to the electrostatic potential from which electrostatic energies can be determined (Fogolari et al., 2002). Formally, the PB equation is a second-order partial differential equation:

$$-\nabla \cdot [\varepsilon(r)\nabla\phi(r)] + \varepsilon(r)\kappa^2(r)\sinh[\phi(r)] = \frac{e}{k_B T} 4\pi\rho(r), \quad (1)$$

where $\varphi = e\Phi/k_BT$ is the reduced electrostatic potential, ε is the dielectric value of the different spatial regions (water, membrane, protein), κ is the Debye-Hückel screening parameter related to the ionic conditions of the solvent, ρ is the spatial distribution of the fixed charges on the protein, and r is the position in three dimensional space. This theory has been applied widely to study ligand binding, protein-protein interactions, and conformational change, with the majority of the studies aimed at soluble proteins.

Electrostatics play an intimate role in the function of membrane proteins as well, and the low-dielectric nature of the membrane has a large influence on the electric fields and energetics of proteins and small molecules at or near the lipid bilayer. Key studies have used PB theory to determine the protonation state of residues in membrane spanning regions (Bashford and Gerwert, 1992; Karshikoff et al., 1994), the insertion energetics of hydrophobic helices (Ben-Tal et al., 1996), the influence of the membrane potential on transmembrane proteins (Roux, 1997), and how the membrane alters the electrostatic potential experienced by ions passing through channels (Roux and MacKinnon, 1999). While there are several PB solvers available for studying soluble proteins, few have been adapted to explore the influence of the membrane. Previously, we developed the APBSmem software to enable users to carry out a number of calculations relevant to specific membrane processes (Callenberg et al., 2010). APBSmem uses the Adaptive Poisson-Boltzmann Solver (APBS), an open-source finite difference PB solver, as the back-end for its electrostatics calculations (Baker et al., 2001).

Here, we report a number of significant advances to APBSmem that make it more versatile, providing additional energetic information for users, increased protein and membrane manipulation, bundling with PDB2PQR for pK_a calculations, and the ability to report non-polar energy values, which are needed to better model membrane protein stability. A number of these additions are shown in **Figure 1** and are discussed in detail in the Experimental Procedures and Supplemental Information. We demonstrate the new features of APBSmem through five case studies. The first two cases explore permeation of cations through the recently solved structure of the thermosensitive channel TRPV1. APBSmem automatically identifies residues known to influence conduction, and it provides a rationale for pH dependent changes in ion selectivity. Case III shows how the software can be used to quickly identify residues whose protonation states are altered by the membrane, and Case IV explores properties revealed from a scan of electrostatic insertion energies for all multipass

membrane proteins of known structure. Finally, Case V shows how protein stability and orientation in the membrane can be predicted with a simple model based on non-polar energetics coupled with electrostatics.

RESULTS

Case I: Ion & small molecule placement and manipulation for computing electrostatic energy profiles

Due to the low-dielectric nature of the lipid bilayer, ions and small charged molecules cannot readily cross the membranes of cells and organelles. Instead, ion channels and transporters span membranes to facilitate movement. Since ions and many small molecules are electrically charged, electrostatic interactions with the channel or transporter are key determinants of the magnitude of the flux and substrate selectivity. Previously, we demonstrated the ease with which APBSmem can be used to calculate the electrostatic solvation free energy of potassium ions in the pore of the membrane-embedded KcsA potassium channel (Callenberg et al., 2010) by revisiting the seminal study on this topic by Roux and MacKinnon (Roux and MacKinnon, 1999). The ion transfer free energy, ΔG_{elec}, is calculated as:

$$\Delta G_{elec} = E_{P,I} - E_P - E_I, \quad (2)$$

where $E_{P,I}$ is the electrostatic energy of the protein plus ion embedded in the membrane, E_P is the energy of the protein in the membrane, and E_I is the energy of the ion in solution. A description of how total electrostatic energies (as in Eq. 2) are computed from Eq. 1 is presented in the Supplemental Information. Unfortunately, there are still several major hurdles to carrying out these calculations that make them difficult for non-experts including charge assignments, orienting the protein in the membrane, editing the dielectric around the protein to include the influence of the membrane, and then placing and moving ions through pathways of interest. We have added features to APBSmem that streamline these steps (**Figure 1**).

We examine ion movement through TRPV1, a narrow channel that is selective for Ca^{2+} and to a lesser degree for Na^{+} (Caterina et al., 1997). TRPV1 is thermosensitive, mildly voltage dependent, and sensitive to several toxins and irritants such as capsaicin, which is the active ingredient in chili peppers (Caterina et al., 1997). The channel is a tetramer with each subunit having 6 transmembrane (TM) segments, and the last two TMs form the central pore domain through which ions flow (A). The pore has two constriction zones: one at the selectivity filter composed of residues GMGD and a second hydrophobic gate near the cytoplasmic side of the membrane where the TM6 helices cross (Liao et al., 2013). TRPV1 agonists can induce large conformal changes, opening one or both gates (Cao et al., 2013). The most open conformation of the channel was recently determined via electron cryo-microscopy in the presence of a vanilloid agonist resiniferatoxin (RTX) and double-knot toxin (DkTx) (Cao et al., 2013; Liao et al., 2013).

The channel structure (PDB ID: 3j5q) was loaded into APBSmem and then new features in the ***Orient*** menu were used to translate the channel −20 Å along the z-axis, rotate by 180°

about the x-axis, followed by a 45° rotation about the z-axis. Next, we chose a smoothed molecular surface representation for the protein (Nina et al., 1997), and the SWANSON parameter set for the atomic radii and charges (Swanson et al., 2007), since the dielectric smoothing inherent in this method generally gives rise to non-rugged ion energy profiles. Parameterizing the pdb file to create what is known as a pqr file is quite easy now that we have bundled PDB2PQR into the APBSmem distribution (Dolinsky et al., 2004). For Cases III-V, we will use the PARSE charge and radii set to parameterize the proteins since that model was specifically developed to explore the free energy of partitioning between aqueous and non-polar environments (Sitkoff et al., 1994). The upper and lower boundaries of the membrane must be set by hand in the graphical user interface (GUI) for the protein of interest (**Figure** 1), and then APBSmem edits the local dielectric, charge, and ion accessibility around the protein to include the presence of the membrane for electrostatics calculations. The presence of aqueous cavities makes it difficult to unambiguously identify the membrane-protein boundaries when adding the membrane. This task is particularly difficult for channels containing fenestrations that connect the inner pore directly to the mid-plane of the bilayer, such as the voltage-gated sodium channels (Payandeh et al., 2012; Shaya et al., 2014; Zhang et al., 2012) (**Figure** 2B). Programs exist for detecting cavities in proteins (Smart et al., 1996; Voss and Gerstein, 2010); however, detection can also be difficult when the water pathways are convoluted and the protein lacks symmetry, in which case more computationally demanding methods are needed (Adelman et al., 2014). To this end, we use a six-way flood-filling method illustrated in **Figure** 2A, which starts from a 'seed' point known to be within the membrane and then tests surrounding regions to determine if they are within the membrane boundaries and external to the protein. The entire membrane is drawn by expanding from this seed in an iterative manner. An additional threshold can be set that prevents expansion into holes smaller than a vertical thickness of t (**Figure** 2B). Here, we use a value of t equal 8 Å, which roughly approximates the size of a lipid molecule, and this value successfully allows for the proper identification of aqueous cavities.

The final membrane embedded protein is shown in **Figure 3**A with the corresponding membrane boundaries. We then used the new ***Ion/Step ion*** function to create a Ca^{2+} ion and move it along the z-axis through the center of the pore from −40 to +80 Å. A series of calculations were initiated along the path to determine the electrostatic component of the free energy, ΔG_{elec} in Eq. 2, for each position (**Figure 3**B). Parameter values for all calculations are listed in **Table 1**. The energy profile is marked by asterisks corresponding to locations of interest, and the positions were also identified on the structure (from top to bottom): two minima in the selectivity filter, one minimum in the central cavity between both gates, and one location near the lower gate. These positions most likely reveal regions of the channel involved in selectivity or function, which we explore in more detail in Case II. Additional technical aspects of the calculation concerning timings, the choice of molecular surfaces, linear versus non-linear solutions, and grid spacing are discussed in the Supplemental Information.

Case II: Contribution of individual residues to the electrostatic interaction

Specific residues often play a crucial role in determining protein function by stabilizing bound ligands, facilitating ion permeation, or providing structural integrity through salt bridge interactions. While several phenomena contribute to stabilization, electrostatics is often a key factor, and in some cases it can be the dominant term. With this in mind, it is useful to determine the contribution of a particular residue to an electrostatic interaction, and this information can help interpret structural information to guide future experiments, as reported by Robertson and colleagues in their work on inward rectifier channels (Robertson et al., 2008). The technical details for isolating electrostatic interaction energies between ions or small molecules with specific residues in a protein can be found in the Experimental Procedures and Supplemental Information.

Here, we highlight the utility of APBSmem's ability to dissect the electrostatic contribution of each residue by reexamining Ca^{2+} permeation through TRPV1. As described in Case I, the ion experiences energy minima at four locations in the channel (asterisks in **Figure 3**B), and we identified the top five amino acids that interact most strongly with the ion at each of these positions (vertical dashed lines in **Figure 4**A-D). The interaction energy of these residues with the ion is plotted throughout the channel to reveal the spatial extent of their influence. The channel with the ions (red) at each of the four positions is shown to the right of each profile. Not surprisingly, charged residues contribute the most to the electrostatic interaction energy. However, this is not always the case as the carbonyl group of G643 plays an important role in stabilizing the cation in the narrow portion of the filter (panel B), which is observed for potassium channels. The ease with which APBSmem identifies these crucial residues through these calculations provides a convenient and rational means to select targets for mutational and functional studies.

Many of the residues in **Figure 4** were previously shown to play a role in conduction. Counterintuitively, Liu and coworkers demonstrated that a basic residue, K639, is essential for cation conduction, and neutralization (i.e., K639Q) reduces current (Liu et al., 2009a). Our calculations reveal that K639 destabilizes permeating ions more than any other residue in the channel, offsetting the deep energy well created by acidic amino acids that would otherwise trap Ca^{2+}. This result supports the hypothesis that decreased single channel conductance in the K639Q channel results from longer Ca^{2+} dwell times in the primary binding sites. Stabilization in the selectivity filter is dominated by D646, E636 and to a lesser extent E648 (panels A and B). Indeed, mutations that neutralize D646, E648 and E651 reduce Ca^{2+} permeability (Chung et al., 2008; Garcia-Martinez et al., 2000; Samways et al., 2008; Welch et al., 2000), and result in a loss of Ca^{2+} selectivity with respect to Na^{+} (Samways et al., 2008). A more recent study showed that D646, E648, and E651 provide a strong Ca^{2+} binding site (Samways and Egan, 2011), which is in agreement with the deep electrostatic well shown in **Figure 3**B, but APBSmem does not reveal an electrostatic role for E651. Unlike the other acidic residues, E636Q causes a significant increase in the agonist induced fraction of total current carried by Ca^{2+} (Samways and Egan, 2011). It is often difficult to determine the kinetic properties of a channel, such as conduction rate and non-equilibrium selectivity, from equilibrium free energy profiles. However, these profiles can be coupled with simple kinetic models to reveal estimates of single channel flux and

differential flux for different ions, thus providing deeper mechanistic insight into how residues control channel properties.

Data suggest the existence of an ion-binding site deeper in the pore than the ones stabilized by D646/E648/E651 in the filter (Chung et al., 2008). Our calculations show that the minimum in the central cavity at 17.6 Å is slightly more stable than the other sites, and the top contributor at this position is D576 (panel C). Previously, the charge at this position was recognized as being important for capsaicin-dependent activation (Boukalova et al., 2010), but to our knowledge, its importance in ion stabilization had gone unnoticed. We suggest that mutations at D576 may change channel conduction properties. Together, APBSmem provides an automated pipeline to gain inferences about new protein structures in which critical residues may not yet have been identified.

Next, we explored the influence that the protonation state of particular acidic residues had on the very stable energy profiles in **Figure 3**B. Using patch clamp photometry and site-directed mutagenesis, Samways and co-workers demonstrated that protonation of residues D646, E648 and E651 significantly reduces the fraction of total current carried by Ca^{2+} in a manner indistinguishable from pH-dependent loss of selectivity (Samways et al., 2008), hinting at a mechanism for pH-dependent loss of Ca^{2+} selectivity in which these residues become protonated. They later estimated that the D646N/E648Q/E651Q triple mutant lacked any selectivity for Ca^{2+} over Na^{+} (Samways and Egan, 2011). Our initial calculation showed that D646 is most important for ion stabilization, and since TRPV1 is a tetramer, there are four copies of this residue. We protonated each in turn and recomputed the corresponding Ca^{2+} and Na^{+} profiles. To facilitate such calculations, we created a dialog box so that charge states for individual residues can be set prior to each calculation using the integrated PROPKA plugin (Li et al., 2005; Olsson et al., 2011). In the ***Assign charge states*** section of the GUI a button exists to select any amino acid in the protein identifying them by their chemical name, residue number, and chain ID.

Neutralization of all four D646 residues results in a 6.8 kcal/mol decrease in Ca^{2+} binding energy at the most extracellular site (32.0 Å) and an extracellular shift in the position (**Figure 5**A). The sites at 24.8 Å and 17.6 Å are also destabilized, but by a much smaller amount: 4 and 0.4 kcal/mol, respectively. Protonation changes in the protein can therefore dramatically influence binding energy and ion dwell times at positions along the pore. Additionally, we carried out the electrostatic free energy calculations on a sodium-like cation (**Figure 5**B). Even when all four D646 residues are charged, the binding energy is much smaller due to sodium's reduced valency, and the most extracellular site is barely present. Correspondingly, protonating D646 has less of an impact on the energy profile, and a rough comparison of the binding energy changes at each site reveal an energy difference between Ca^{2+} and Na^{+} of −4.5, −2.3 and −3.7 kcal/mol prior to protonation and 1.7, 0.4 and −3.4 kcal/mol after full protonation at the extracellular filter site, intracellular filter site, and the cavity site, respectively (**Figure 5**C). Thus, the electrostatic changes alone show a dramatic loss of binding energy for Ca^{2+} compared to Na^{+} when the filter sites are protonated in response to a drop in pH. These calculations corroborate the loss of selectivity as the pH decreases, as reported (Chung et al., 2008; Samways and Egan, 2011; Samways et al., 2008).

Case III: Determination of membrane induced pK_a shifts

The protonation state of a residue can be influenced by the local electrical environment, changes in pH (as discussed in Case II), and the dielectric environment. There is significant literature centered on the use of continuum electrostatics for predicting pK_a shifts of residues since charge changes can impact protein structure, ligand binding, and protein-protein interactions, see (Alexov et al., 2011), and earlier studies have used solutions to the PB equation to explore pK_a shifts in the presence of the membrane for membrane proteins such as bacteriodopson (Bashford and Gerwert, 1992) and outer-membrane porins (Karshikoff et al., 1994). When a charged group moves from a high-dielectric environment, like water, into a low-dielectric medium, such as the bilayer core, there is an electrostatic penalty, which can be thought of as the energy associated with stripping away polar water molecules from the protein. Neutralizing the residue can mitigate this energetic cost, and if the resulting energy decrease is greater than the free energy of ionization, then the group will likely be neutral in the membrane. As shown in Figure S1, we calculate these shifts using two thermodynamic cycles for de/protonation of a residue of interest in solution (ΔpK_a^1, cycle 1) and a cycle corresponding to a change in charge state in the membrane (ΔpK_a^2, cycle 2). PROPKA is used to compute the shift along cycle 1 (Li et al., 2005; Olsson et al., 2011), and APBSmem is used to estimate the shift due to the membrane using the PB approach developed by Honig and co-workers (Yang et al., 1993) as described in the Supplemental Information. Thus, the pK_a of a residue is given by:

$$pK_a = pK_a^0 + \Delta pK_a^1 + \Delta pK_a^2, \quad (3)$$

where pK_a^0 is the experimentally determined pK_a of the isolated residue. APBSmem will calculate the ΔpK_a of a single residue, or it will provide a rank ordered list of residues most likely to be shifted based on a single, heuristic approximation presented next.

Here, we demonstrate APBSmem's ΔpK_a calculator with mVDAC1 and LeuT for which timings and memory usage can be found in **Table S1**. As an initial evaluation, we ran a single solvation energy calculation for mVDAC1 with all residues set to standard protonation states at pH 7 to obtain the per-residue components of the solvation energy (**Figure 6**A). For these calculations, we subtract the total fixed charge energy of mVDAC1 in solution from the membrane embedded value and report the per-residue contribution. While not a direct indicator of ΔpK_a, large energy values might be reduced if the residue is neutralized. This quick calculation singled out E73 and K110 as having the largest solvation energies. The side chain of E73 is oriented towards the hydrophobic core of the membrane, as suggested earlier by De Pinto and co-workers (De Pinto et al., 1993), while K110 points toward the bilayer at the headgroup-core interface (**Figure 6**C). **Figure 6**B shows membrane induced residue pK_a shifts for all R, K, D, E, Y, and C residues in mVDAC1 (ΔpK_a^2), assuming a protein dielectric of 2 and 8 since it is often debated which dielectric value is most appropriate (Kukic et al., 2013). As predicted by the fixed energy solvation values, both E73 and K110 have the most profound shifts, regardless of the protein dielectric constant employed. The modified pK_a of E73 and K110 are 25.37 and −0.87, respectively (**Table 2**). Values above 7 indicate protonation at neutral pH, while values less than 7 indicate a lack of protonation; thus, we predict that K110 and E73 are both neutral. Our

findings corroborate recent MD simulations showing that E73 causes bending and water penetration into the membrane when charged (Villinger et al., 2010). However, simulations have not reported deprotonation of K110 (Choudhary et al., 2014; Noskov et al., 2013; Rui et al., 2011; Villinger et al., 2010) potentially due to electrostatic compensation due to snorkeling into the headgroups.

The per-residue solvation energies for the LeuT transporter reveal that K288 is an outlier (**Figure 6**D). The membrane induced pK_a shift is −12.64 (**Figure 6**E), indicating that it is most likely neutral and which is consistent with its position in the bilayer core (**Figure 6**F). Not surprisingly MD simulations with K288 charged result in membrane deformations, water penetration, and membrane thinning at the site (Mondal et al., 2013; Mondal et al., 2014), and these deformations could help keep the residue charged (Callenberg et al., 2012; Li et al., 2008; Mondal et al., 2013; Mondal et al., 2014; Yoo and Cui, 2008).

We want to emphasize that the membrane-induced pK_a shifts described here are a first order approximation of a more complete statistical-mechanical treatment, which accounts for the interaction of multiple charged sites in all possible ionization configurations (Yang et al., 1993). This full treatment can be done using the shell scripting feature with APBSmem, but except for the smallest proteins, this calculation can be extremely time consuming; thus, it is useful to consider solving this problem with approximate methods (Bashford and Karplus, 1991; Tanford and Roxby, 1972), or Monte Carlo-based approaches (Beroza et al., 1991). Furthermore, charged side chains are often able to reduce their electrostatic penalty either by snorkeling into the head group region, or by forming hydrogen bonds with nearby residues that would otherwise not form if the protein were in aqueous solution. Thus, in addition to exploring the full ensemble of possible titration states, one would also need to optimize side chain conformations in order to obtain a more accurate pK_a.

Case IV: Electrostatic survey of membrane proteins of known structure

We combined the automatic membrane detection algorithm with command line scripting to expand our per-residue solvation energy analysis to 1,614 multi-pass membrane proteins available in the OPM database (Lomize et al., 2006). For each protein, we identified residues that incurred a 10 kcal/mol or greater electrostatic penalty for residing in the membrane, assuming standard protonation states at pH 7. We used the membrane thicknesses determined by OPM for each protein. While most membrane proteins have no residues (41%) or one residue (15%) in violation, APBSmem identified 707 proteins that have 5 or more residues in violation (44%). For instance, the method correctly identified all 12 copies of the titratable rotor site (D61) on the rotor domain of the F_O-ATPase (PDB ID: 1c17), whose protonation is crucial for ion transport (Rastogi and Girvin, 1999). In Figure 7A, we picture three of the top five structures with the most violations: the KvAP voltage-gated potassium channel (PDB ID: 2a0l, (Jiang et al., 2003)) with 52 penalties, the capsaicin-bound TRPV1 channel (PDB ID: 3j5r, (Liao et al., 2013)) with 25 penalties, and the mechanosensitive channel of large conductance MscL (PDB ID: 3hzq, (Liu et al., 2009b)), with 24 penalties. The physiological relevance of the KvAP structure is not clear (Cohen et al., 2003) and many of the high energy residues are buried deep in what would be the core of the membrane, but offending residues are located near the headgroup interface

for both MscL and TRPV1. It is possible that minor membrane bending could accommodate the residual hydrophobic mismatch for these proteins. In the future, we will explore membrane bending effects with our implicit membrane-bending model (Callenberg et al., 2012).

We next categorized the proteins by family using the Mpstruct database (http://blanco.biomol.uci.edu/mpstruct). Figure 7B shows the proportion of α-helical structures evaluated that had at least five residues with electrostatic insertion penalties above 10 kcal/mol for the top twenty families. The majority of these groups are transporters and ion channels, but we also identified families involved in the electron transport chain and light harvesting. For example, APBSmem indicates large penalties for E78 and R207 in cytochrome b6f, which line the proton transfer pathway (Hasan et al., 2013). Thus, α-helical proteins that move charge across membranes appear to have an increased number of charged residues in the transmembrane region that are energetically costly. In contrast, β-barrel proteins generally have fewer residues with large electrostatic penalties. However, many of these proteins also facilitate charge movement, and we hypothesize that the large water filled cavities found in porins reduce the electrostatic fields and corresponding energy penalties. Only the PagP outer membrane palimitoyl transferase (PDB ID: 1mm4, (Hwang et al., 2002)) returned five or more high-energy residues, and these residues are located on the loops of the barrel and at the head group-core interfaces. We found only a very weak correlation ($R^2 < 0.1$) between the resolution of the structures and the number of electrostatically unfavorable residues for α-helical proteins, and there was no correlation for β-barrels (**Figure S2**A-E). That said, the five structures with the highest number of reported residues have resolutions greater than 3.2 Å.

Finally, we categorized the total number of residues with large electrostatic insertion penalties for both α-helical (Figure 7C) and β-barrel (Figure 7D) proteins. As expected, the majority of identified residues are charged, and α-helical proteins contain more basic residues while the most prevalent residue in β-barrels is aspartate. Clearly, many of these residues will be neutralized in the membrane, but we note that some residues we identified are not titratable. For example, the backbone of residue S2 in mitochondrial cytochrome c oxidase (PDB ID: 2zxw, (Aoyama et al., 2009)) is exposed to the membrane core, giving the residue an electrostatic penalty of 11.0 kcal/mol. **Table S2** contains the full list of residues with large solvation energy penalties greater than or equal to 10 kcal/mol, and details on the calculations can be found in the Supplemental Information.

Case V: Prediction of membrane protein insertion energies

Next, we use APBSmem to explore the stability of proteins in the membrane. There are several computational methods available to quantitatively assess the energy of partitioning from water into the membrane, including computational expensive fully atomistic MD simulations (Dorairaj and Allen, 2007; MacCallum et al., 2007), more tractable physics based approaches (Ben-Tal et al., 1996; Lomize et al., 2006), and statistical potentials (Bernsel et al., 2008; Schramm et al., 2012). We employ the method outlined by Honig and co-workers, which assumes that the non-polar energy of insertion (ΔE_{np}) is proportional to the surface area of the molecule (Sitkoff et al., 1994):

$$\Delta E_{np} = a \cdot (A_{mem} - A_{sol}), \quad (4)$$

where A_{mem} is the solvent accessible surface area (SASA) of the protein or molecule in the membrane and A_{sol} is the SASA in solution, and a = 0.028 kcal/mol/Å^2 is a constant of proportionality. Both areas are calculated by APBSmem using a call to the external program MSMS (Sanner et al., 1996), which must be separately downloaded and installed locally. APBSmem includes three models for calculating ΔE_{np}: 1) all surface atoms between the upper and lower leaflets are included in the calculation of A_{mem}, 2) only atoms in the hydrophobic core of the membrane are included, or 3) the constant a in the headgroup regions is linearly scaled from 0.28 kcal/mol/Å^2 to zero as the z-position of a buried atom approaches the membrane-water interface from the headgroup-core interface. The later model is consistent with the observation that water penetration falls off linearly in the headgroup region (Nagle and Tristram-Nagle, 2000), and this is the model we employ here.

Predicting the relative stability of membrane-spanning domains is critical to understand the balance between membrane protein biosynthesis and quality control. As integral membrane proteins are translated and inserted into the endoplasmic reticulum (ER), their TMs must adopt the proper topology and interact correctly with subsequent TMs to ensure native folding and function (Skach, 2009). Failure to fold can result in protein destruction by ER-associated degradation (ERAD), a quality control pathway that triages misfolded proteins (Needham and Brodsky, 2013). Folding of multi-pass membrane proteins is highly problematic due to the number of membrane spanning domains and the complexity of intermembrane interactions, especially for ATP binding cassette (ABC) transporters, which possess 12 TMs and two large cytoplasmic nucleotide binding domains (NBDs). Indeed, destabilizing mutations within ABC transporters lead to a number of diseases (Guerriero and Brodsky, 2012).

A model misfolded ABC transporter is a truncated form of the yeast mating pheromone transporter Sterile 6 (Ste6p*). Following translation, wild type Ste6p* traffics to the plasma membrane; however, a 42 amino acid truncation in the second NBD (NBD2) results in ER retention and destruction by the ERAD pathway (Loayza et al., 1998). To model ABC transporter TM insertion, folding, and quality control, we created an internal deletion of Ste6p* to remove all but the first two TMs, which were then appended to the truncated NBD2. This species was termed Chimera N*. When expressed in yeast cells, the native TM2 in Chimera N* fails to partition into the membrane (data not shown). However, proper topology is corrected by substitution of TM2 with an artificial poly-A/L hydrophobic stretch offset by helix terminating linkers (Hessa et al., 2007) (Figure 8).

Because a high resolution structure of Ste6p* is lacking, we created a homology model of the wild type and mutant constructs based on the related P-glycoprotein (P-gp) ABC transporter (PDB ID: 3g5u, 26% identity, (Aller et al., 2009)) (see Supplement Information and **Figure S3** for details on model construction). Superposing the 2TM model of Ste6p* (yellow) on the P-gp transporter (green) reveals that both helices have extensive interactions with other TM segments (Figure 8A), which may explain why Chimera N* fails to adopt the correct topology. To explore the energetic stability of the isolated wild type and artificial

hydrophobic TM2 segments, we calculated the sum of the non-polar (Eq. 4) and electrostatic energies (from Eq. 1) for each segment at different positions in the membrane, and with each compared to their respective value in solution. We used command line scripting to rotate each segment through a wide range of positions, including fully transmembrane, titled, and interfacial configurations with the hypothesis that the native TM2 sequence may be predisposed to adopt an interfacial configuration, while the engineered TM2 may be more stable in the fully inserted state. An energetic heat map was created for each helix by rotating 360° along the long axis (φ) and then pivoting the helix from 0 to 90° with respect to the membran e normal (θ) while pinning the N-terminus as shown in panel B. See the Supplemental Information for a complete description of the electrostatic energy and scripting.

As hypothesized, the native TM2 is significantly more stable bound to the membrane than in aqueous solution with nearly equal values in interfacial (−35 kcal/mol) and transmembrane configurations (−36 kcal/mol). The overall stability in or near the membrane is not surprising given the hydrophobic character of the primary sequence, and the similarity between these two energetic values may explain why this segment fails to insert. Meanwhile, the artificial hydrophobic TM2 segment is more stable in the transmembrane (−43 kcal/mol) than the interfacial configuration (−33 kcal/mol) due to the poly-A/L sequence. The 10 kcal/mol increased stability of the transmembrane configuration likely explains its correct topological insertion.

DISCUSSION

We have explored a diverse set of biological problems related to the electrostatics and stability of membrane proteins. In doing so, we used several new features of the APBSmem software that significantly enhance its usability and power. The ability to manipulate protein orientation and position coupled with the bundling of PDB2PQR now makes it possible to initiate calculations entirely within APBSmem directly from a PDB file without the use of external software packages. Added functionality for ion placement and movement allows users to easily explore the electrostatics of ion movement through channels. Moreover, increased handling of energetic terms makes it possible to extract specific interactions between protein residues and ions or small molecules in the system, which helps identify amino acids critical to permeation or binding. We also developed a scheme to determine the membrane-induced shifts in residue pK_a values in combination with existing methods in the incorporated PROPKA software. Using newly added command line scripting, we compiled a comprehensive list of residues likely to have altered protonation states for all integral membrane proteins in the OPM database. Finally, a more complete model of membrane protein stability that includes non-polar energies can now be calculated with APBSmem, since it interfaces with the program MSMS. While other energetic terms such as protein conformational change, entropy, and membrane distortions are ignored, non-polar and electrostatic energies alone can provide a first approximation to protein stability. Thus, the ease and speed of APBSmem coupled with its ability to predict changes at the single amino acid level make it a first line approach for exploring the stability of membrane and membrane-associated proteins.

Throughout this study we have assumed that the membrane remains flat and undeformed, and there are instances where this will not be true. An ongoing effort in our lab is to incorporate membrane deformations into a continuum framework consistent with APBSmem (Callenberg et al., 2012), and future releases will include this feature. Additionally, the parameters listed in **Table 1** are based on typical continuum electrostatics calculations. For example, the high dielectric value of 80 used in the head groups is inspired by fully atomistic simulations carried out in the Feller lab (Stern and Feller, 2003), but they are not intended to be applicable to all situations. The APBSmem GUI makes it easy for researchers to explore different values. In particular, it will be interesting to use APBSmem with the flexibility provided through batch scripting to benchmark known pK_a shifts for membrane protein residues to identify optimal model parameters and test quantitative aspects of our method.

The latest free software version of APBSmem can be downloaded from http://apbsmem.sourceforge.net.

EXPERIMENTAL PROCEDURES

All calculations were carried out with APBSmem, which is a Java-based program that aids in solving the PB equation in the presence of membrane-like environments. It can be run from a GUI or from the command line using pre-specified input files. PDB files were loaded into the software, and charge models were set using the bundled PDB2PQR package. Non-standard protonation states of specific residues were assigned with PROPKA, which is also now bundled with APBSmem. Through the GUI interface calculation parameters were set including calculation type (ion solvation energy, gating charge/voltage dependence calculations, membrane insertion energy, pK_a shifts, etc.), spatial dimensions and grid discretization, membrane/protein/solution dielectric values, protein surface representation, far-field boundary conditions, as well as other parameters typical of molecular PB calculations. Once all parameters are set, APBSmem calls APBS to generate an initial dielectric environment map (ε), ion accessibility map (κ) and explicit charge map (ρ) based on the molecular coordinates and any explicit ions in solution. These maps are then manipulated by APBSmem to include the presence of an implicit membrane in the dielectric and ion accessibility maps, as well as the charge maps if a membrane potential is imposed on the system. The ***Preview*** button allows the user to quickly visualize the protein's placement in the membrane, which is crucial at this stage to ensure proper orientation in the membrane with the desired membrane-protein boundaries. APBSmem next calls on APBS again using the altered maps to numerically solve the PB equation in Eq. 1. This flow makes APBSmem operation transparent: after an APBSmem calculation, calculations can be repeated without using APBSmem by simply running APBS on the generated input files. An in-depth discussion of the basic features of the software is provided in our original manuscript (Callenberg et al., 2010).

Per-residue solvation energies in **Figures 6** and **7** are calculated as the sum of the fixed-charge energies for all residue atoms computed in the presence of the membrane subtracted from the fixed-charge energy when the protein is in solution. Per-residue ion interaction energies are calculated by summing the per-atom fixed-charge energies over each atom in a

residue. This energy value is formally divergent because it evaluates the potential at the position of the atoms, so APBSmem isolates the residue-ion interaction energy by subtracting off the protein-protein energies. These per-residue interaction energies are saved to a log file in the output directory and used to produce the curves in **Figure 4**.

pK_a shifts are calculated from a set of thermodynamic cycles. We consider two cycles: first, the energy required to protonate/deprotonate the residue of interest in solution (cycle 1), and second, the energy required to protonate/deprotonate the residue in the presence of the membrane (cycle 2). We use PROPKA to compute the values along cycle 1. APBSmem solves the PB equation to determine the change in total electrostatic energy for inserting a protein into the membrane with the residue deprotonated and the change in energy with the residue protonated. This difference between these energies is used to calculate the shift in pK_a along cycle 2. Details of these cycles are further described in **Figure S1** and the Supplemental Information.

Homology models of the transmembrane domains (TM1 & TM2) of the ATP-binding cassette (ABC) transporter Ste6p* described in case V were constructed with Modeller9v13 (Sali and Blundell, 1993) using the P-glycoprotein transporter (PDB ID: 3g5u) as a template structure and the alignment provided in **Figure S3**. Additional hand adjustments were then carried out to close up gaps and maximally align the second transmembrane regions. The final alignment used for construction of the first two TM segments of Ste6p* and the wild-type TM2 segment is shown in **Figure S3**. The mutant TM2 segment was then constructed using the wild-type TM2 model as a template. Please note that for the TM insertion energy calculations, these alignments are not crucial since we simply assume that both TM2 segments take on roughly straight helical configurations.

The new features added to APBSmem that are used throughout this study are more fully described in the Supplemental Information and include: enhanced PDB/PQR file processing, greater geometric control over proteins, ions and small molecules, automatic identification of the membrane, non-polar energy calculations with MSMS, per-residue contributions to energies, command line scripting, and ligand solvation energy calculations.

Supplementary Material

Refer to Web version on PubMed Central for supplementary material.

ACKNOWLEDGEMENTS

We thank Keith Callenberg and Naomi Latorraca for their help in this project, and Marco Lolicato for his help testing the software. We also thank Nathan Baker and Keith Star for continued support concerning the integration of APBSmem and APBS. Finally, we thank Yifan Cheng for his helpful discussions concerning the electrostatic calculations on TRPV1. This work was funded by NSF CAREER award MCB-0845286 (M.G.), NIH grant DK101584 (C.J.G.), and NIH grants GM75061 and DK79307 (J.L.B.).

REFERENCES

Adelman JL, Sheng Y, Choe S, Abramson J, Wright EM, Rosenberg JM, Grabe M. Structural determinants of water permeation through the sodium-galactose transporter vSGLT. Biophys. J. 2014; 106:1280–1289. [PubMed: 24655503]

Alexov E, Mehler EL, Baker N, Baptista AM, Huang Y, Milletti F, Nielsen JE, Farrell D, Carstensen T, Olsson MH, et al. Progress in the prediction of pKa values in proteins. Proteins. 2011; 79:3260–3275. [PubMed: 22002859]

Aller SG, Yu J, Ward A, Weng Y, Chittaboina S, Zhuo R, Harrell PM, Trinh YT, Zhang Q, Urbatsch IL, et al. Structure of P-glycoprotein reveals a molecular basis for poly-specific drug binding. Science. 2009; 323:1718–1722. [PubMed: 19325113]

Aoyama H, Muramoto K, Shinzawa-Itoh K, Hirata K, Yamashita E, Tsukihara T, Ogura T, Yoshikawa S. A peroxide bridge between Fe and Cu ions in the O2 reduction site of fully oxidized cytochrome c oxidase could suppress the proton pump. Proceedings of the National Academy of Sciences of the United States of America. 2009; 106:2165–2169. [PubMed: 19164527]

Baker NA, Sept D, Joseph S, Holst MJ, McCammon JA. Electrostatics of nanosystems: application to microtubules and the ribosome. Proc. Natl. Acad. Sci. USA. 2001; 98:10037–10041. [PubMed: 11517324]

Bashford D, Gerwert K. Electrostatic calculations of the pKa values of ionizable groups in bacteriorhodopsin. Journal of molecular biology. 1992; 224:473–486. [PubMed: 1313886]

Bashford D, Karplus M. Multiple-Site Titration Curves of Proteins - an Analysis of Exact and Approximate Methods for Their Calculation. J Phys Chem-Us. 1991; 95:9556–9561.

Ben-Tal N, Ben-Shaul A, Nicholls A, Honig B. Free-energy determinants of alpha-helix insertion into lipid bilayers. Biophys. J. 1996; 70:1803–1812. [PubMed: 8785340]

Bernsel A, Viklund H, Falk J, Lindahl E, von Heijne G, Elofsson A. Prediction of membrane-protein topology from first principles. Proc. Natl. Acad. Sci. USA. 2008; 105:7177–7181. [PubMed: 18477697]

Beroza P, Fredkin DR, Okamura MY, Feher G. Protonation of interacting residues in a protein by a Monte Carlo method: application to lysozyme and the photosynthetic reaction center of Rhodobacter sphaeroides. Proceedings of the National Academy of Sciences of the United States of America. 1991; 88:5804–5808. [PubMed: 2062860]

Boukalova S, Marsakova L, Teisinger J, Vlachova V. Conserved residues within the putative S4-S5 region serve distinct functions among thermosensitive vanilloid transient receptor potential (TRPV) channels. J. Biol. Chem. 2010; 285:41455–41462. [PubMed: 21044960]

Brooks BR, Brooks CL 3rd, Mackerell AD Jr. Nilsson L, Petrella RJ, Roux B, Won Y, Archontis G, Bartels C, Boresch S, et al. CHARMM: the biomolecular simulation program. J. Comput. Chem. 2009; 30:1545–1614. [PubMed: 19444816]

Callenberg KM, Choudhary OP, de Forest GL, Gohara DW, Baker NA, Grabe M. APBSmem: a graphical interface for electrostatic calculations at the membrane. PloS one. 2010; 5

Callenberg KM, Latorraca NR, Grabe M. Membrane bending is critical for the stability of voltage sensor segments in the membrane. J. Gen. Physiol. 2012; 140:55–68. [PubMed: 22732310]

Cao E, Liao M, Cheng Y, Julius D. TRPV1 structures in distinct conformations reveal activation mechanisms. Nature. 2013; 504:113–118. [PubMed: 24305161]

Caterina MJ, Schumacher MA, Tominaga M, Rosen TA, Levine JD, Julius D. The capsaicin receptor: a heat-activated ion channel in the pain pathway. Nature. 1997; 389:816–824. [PubMed: 9349813]

Choudhary OP, Paz A, Adelman JL, Colletier JP, Abramson J, Grabe M. Structure-guided simulations illuminate the mechanism of ATP transport through VDAC1. Nat. Struct. Mol. Biol. 2014; 21:626–632. [PubMed: 24908397]

Chung MK, Guler AD, Caterina MJ. TRPV1 shows dynamic ionic selectivity during agonist stimulation. Nat Neurosci. 2008; 11:555–564. [PubMed: 18391945]

Cohen BE, Grabe M, Jan LY. Answers and questions from the KvAP structures. Neuron. 2003; 39:395–400. [PubMed: 12895415]

De Pinto V, al Jamal JA, Palmieri F. Location of the dicyclohexylcarbodiimide-reactive glutamate residue in the bovine heart mitochondrial porin. J. Biol. Chem. 1993; 268:12977–12982. [PubMed: 7685355]

Dolinsky TJ, Nielsen JE, McCammon JA, Baker NA. PDB2PQR: an automated pipeline for the setup of Poisson-Boltzmann electrostatics calculations. Nucleic Acids Res. 2004; 32:W665–667. [PubMed: 15215472]

Dorairaj S, Allen TW. On the thermodynamic stability of a charged arginine side chain in a transmembrane helix. Proc. Natl. Acad. Sci. USA. 2007; 104:4943–4948. [PubMed: 17360368]

Fogolari F, Brigo A, Molinari H. The Poisson-Boltzmann equation for biomolecular electrostatics: a tool for structural biology. J. Mol. Recognit. 2002; 15:377–392. [PubMed: 12501158]

Garcia-Martinez C, Morenilla-Palao C, Planells-Cases R, Merino JM, Ferrer-Montiel A. Identification of an aspartic residue in the P-loop of the vanilloid receptor that modulates pore properties. J. Biol. Chem. 2000; 275:32552–32558. [PubMed: 10931826]

Gilson MK, Honig BH. Calculation of electrostatic potentials in an enzyme active site. Nature. 1987; 330:84–86. [PubMed: 3313058]

Grant JA, Pickup BT, Nicholls A. A smooth permittivity function for Poisson-Boltzmann solvation methods. J. Comput. Chem. 2001; 22:608–640.

Guerriero CJ, Brodsky JL. The delicate balance between secreted protein folding and endoplasmic reticulum-associated degradation in human physiology. Physiological reviews. 2012; 92:537–576. [PubMed: 22535891]

Hasan SS, Yamashita E, Baniulis D, Cramer WA. Quinone-dependent proton transfer pathways in the photosynthetic cytochrome b6f complex. Proceedings of the National Academy of Sciences of the United States of America. 2013; 110:4297–4302. [PubMed: 23440205]

Hessa T, Meindl-Beinker NM, Bernsel A, Kim H, Sato Y, Lerch-Bader M, Nilsson I, White SH, von Heijne G. Molecular code for transmembrane-helix recognition by the Sec61 translocon. Nature. 2007; 450:1026–1032. [PubMed: 18075582]

Hwang PM, Choy WY, Lo EI, Chen L, Forman-Kay JD, Raetz CR, Prive GG, Bishop RE, Kay LE. Solution structure and dynamics of the outer membrane enzyme PagP by NMR. Proceedings of the National Academy of Sciences of the United States of America. 2002; 99:13560–13565. [PubMed: 12357033]

Jiang Y, Lee A, Chen J, Ruta V, Cadene M, Chait BT, MacKinnon R. X-ray structure of a voltage-dependent K+ channel. Nature. 2003; 423:33–41. [PubMed: 12721618]

Karshikoff A, Spassov V, Cowan SW, Ladenstein R, Schirmer T. Electrostatic properties of two porin channels from Escherichia coli. Journal of molecular biology. 1994; 240:372–384. [PubMed: 8035460]

Kukic P, Farrell D, McIntosh LP, Garcia-Moreno EB, Jensen KS, Toleikis Z, Teilum K, Nielsen JE. Protein dielectric constants determined from NMR chemical shift perturbations. J. Am. Chem. Soc. 2013; 135:16968–16976. [PubMed: 24124752]

Li H, Robertson AD, Jensen JH. Very fast empirical prediction and rationalization of protein pKa values. Proteins. 2005; 61:704–721. [PubMed: 16231289]

Li L, Vorobyov I, MacKerell AD Jr, Allen TW. Is arginine charged in a membrane? Biophys. J. 2008; 94:L11–13. [PubMed: 17981901]

Liao M, Cao E, Julius D, Cheng Y. Structure of the TRPV1 ion channel determined by electron cryo-microscopy. Nature. 2013; 504:107–112. [PubMed: 24305160]

Liu B, Yao J, Wang Y, Li H, Qin F. Proton inhibition of unitary currents of vanilloid receptors. J. Gen. Physiol. 2009a; 134:243–258. [PubMed: 19720962]

Liu Z, Gandhi CS, Rees DC. Structure of a tetrameric MscL in an expanded intermediate state. Nature. 2009b; 461:120–124. [PubMed: 19701184]

Loayza D, Tam A, Schmidt WK, Michaelis S. Ste6p mutants defective in exit from the endoplasmic reticulum (ER) reveal aspects of an ER quality control pathway in Saccharomyces cerevisiae. Molecular biology of the cell. 1998; 9:2767–2784. [PubMed: 9763443]

Lomize MA, Lomize AL, Pogozheva ID, Mosberg HI. OPM: orientations of proteins in membranes database. Bioinformatics. 2006; 22:623–625. [PubMed: 16397007]

MacCallum JL, Bennett WF, Tieleman DP. Partitioning of amino acid side chains into lipid bilayers: results from computer simulations and comparison to experiment. J. Gen. Physiol. 2007; 129:371–377. [PubMed: 17438118]

Mondal S, Khelashvili G, Shi L, Weinstein H. The cost of living in the membrane: a case study of hydrophobic mismatch for the multi-segment protein LeuT. Chem. Phys. Lipids. 2013; 169:27–38. [PubMed: 23376428]

Mondal S, Khelashvili G, Weinstein H. Not just an oil slick: how the energetics of protein-membrane interactions impacts the function and organization of transmembrane proteins. Biophys. J. 2014; 106:2305–2316. [PubMed: 24896109]

Nagle JF, Tristram-Nagle S. Structure of lipid bilayers. Biochim. Biophys. Acta. 2000; 1469:159–195. [PubMed: 11063882]

Needham PG, Brodsky JL. How early studies on secreted and membrane protein quality control gave rise to the ER associated degradation (ERAD) pathway: the early history of ERAD. Biochim. Biophys. Acta. 2013; 1833:2447–2457. [PubMed: 23557783]

Nina M, Beglov D, Roux B. Atomic radii for continuum electrostatics calculations based on molecular dynamics free energy simulations. Journal of Physical Chemistry B. 1997; 101:5239–5248.

Noskov SY, Rostovtseva TK, Bezrukov SM. ATP transport through VDAC and the VDAC-tubulin complex probed by equilibrium and nonequilibrium MD simulations. Biochemistry. 2013; 52:9246–9256. [PubMed: 24245503]

Olsson MHM, Sondergaard CR, Rostkowski M, Jensen JH. PROPKA3: Consistent Treatment of Internal and Surface Residues in Empirical pK(a) Predictions. J. Chem. Theory Comput. 2011; 7:525–537.

Payandeh J, Gamal El-Din TM, Scheuer T, Zheng N, Catterall WA. Crystal structure of a voltage-gated sodium channel in two potentially inactivated states. Nature. 2012; 486:135–139. [PubMed: 22678296]

Rastogi VK, Girvin ME. Structural changes linked to proton translocation by subunit c of the ATP synthase. Nature. 1999; 402:263–268. [PubMed: 10580496]

Robertson JL, Palmer LG, Roux B. Long-pore electrostatics in inward-rectifier potassium channels. J. Gen. Physiol. 2008; 132:613–632. [PubMed: 19001143]

Roux B. Influence of the membrane potential on the free energy of an intrinsic protein. Biophys. J. 1997; 73:2980–2989. [PubMed: 9414213]

Roux B, MacKinnon R. The cavity and pore helices in the KcsA K+ channel: electrostatic stabilization of monovalent cations. Science. 1999; 285:100–102. [PubMed: 10390357]

Rui H, Lee KI, Pastor RW, Im W. Molecular dynamics studies of ion permeation in VDAC. Biophys. J. 2011; 100:602–610. [PubMed: 21281574]

Sali A, Blundell TL. Comparative protein modelling by satisfaction of spatial restraints. J. Mol. Biol. 1993; 234:779–815. [PubMed: 8254673]

Samways DS, Egan TM. Calcium-dependent decrease in the single-channel conductance of TRPV1. Pflugers. Arch. 2011; 462:681–691. [PubMed: 21892726]

Samways DS, Khakh BS, Egan TM. Tunable calcium current through TRPV1 receptor channels. J. Biol. Chem. 2008; 283:31274–31278. [PubMed: 18775990]

Sanner MF, Olson AJ, Spehner JC. Reduced surface: an efficient way to compute molecular surfaces. Biopolymers. 1996; 38:305–320. [PubMed: 8906967]

Schramm CA, Hannigan BT, Donald JE, Keasar C, Saven JG, Degrado WF, Samish I. Knowledge-based potential for positioning membrane-associated structures and assessing residue-specific energetic contributions. Structure. 2012; 20:924–935. [PubMed: 22579257]

Shaya D, Findeisen F, Abderemane-Ali F, Arrigoni C, Wong S, Nurva SR, Loussouarn G, Minor DL Jr. Structure of a prokaryotic sodium channel pore reveals essential gating elements and an outer ion binding site common to eukaryotic channels. J. Mol. Biol. 2014; 426:467–483. [PubMed: 24120938]

Sitkoff D, Sharp KA, Honig B. Accurate Calculation of Hydration Free-Energies Using Macroscopic Solvent Models. J. Phys. Chem. 1994; 98:1978–1988.

Skach WR. Cellular mechanisms of membrane protein folding. Nat. Struct. Mol. Biol. 2009; 16:606–612. [PubMed: 19491932]

Smart OS, Neduvelil JG, Wang X, Wallace BA, Sansom MS. HOLE: a program for the analysis of the pore dimensions of ion channel structural models. Journal of molecular graphics. 1996; 14:354–360. [PubMed: 9195488]

Stern HA, Feller SE. Calculation of the dielectric permittivity profile for a nonuniform system: Application to a lipid bilayer simulation. Journal of Chemical Physics. 2003; 118:3401–3412.

Swanson JMJ, Wagoner JA, Baker NA, McCammon JA. Optimizing the Poisson dielectric boundary with explicit solvent forces and energies: Lessons learned with atom-centered dielectric functions. J. Chem. Theory Comp. 2007; 3:170–183.

Tanford C, Roxby R. Interpretation of protein titration curves. Application to lysozyme. Biochemistry. 1972; 11:2192–2198. [PubMed: 5027621]

Villinger S, Briones R, Giller K, Zachariae U, Lange A, de Groot BL, Griesinger C, Becker S, Zweckstetter M. Functional dynamics in the voltage-dependent anion channel. Proc. Natl. Acad. Sci. USA. 2010; 107:22546–22551. [PubMed: 21148773]

Voss NR, Gerstein M. 3V: cavity, channel and cleft volume calculator and extractor. Nucleic Acids Res. 2010; 38:W555–562. [PubMed: 20478824]

Welch JM, Simon SA, Reinhart PH. The activation mechanism of rat vanilloid receptor 1 by capsaicin involves the pore domain and differs from the activation by either acid or heat. Proc. Natl. Acad. Sci. USA. 2000; 97:13889–13894. [PubMed: 11095706]

Yang AS, Gunner MR, Sampogna R, Sharp K, Honig B. On the calculation of pKas in proteins. Proteins. 1993; 15:252–265. [PubMed: 7681210]

Yoo J, Cui Q. Does arginine remain protonated in the lipid membrane? Insights from microscopic pKa calculations. Biophys. J. 2008; 94:L61–63. [PubMed: 18199662]

Zhang X, Ren W, DeCaen P, Yan C, Tao X, Tang L, Wang J, Hasegawa K, Kumasaka T, He J, et al. Crystal structure of an orthologue of the NaChBac voltage-gated sodium channel. Nature. 2012; 486:130–134. [PubMed: 22678295]

Zhou YC, Feig M, Wei GW. Highly accurate biomolecular electrostatics in continuum dielectric environments. J. Comput. Chem. 2008; 29:87–97. [PubMed: 17508411]

Highlights

- Incorporation of PDB2PQR for automated protein preparation
- A new model for determining membrane induced pKa shifts
- First electrostatic analysis on the landmark TRPV1 channel structures
- A survey of the electrostatic properties of 1,614 membrane protein structures

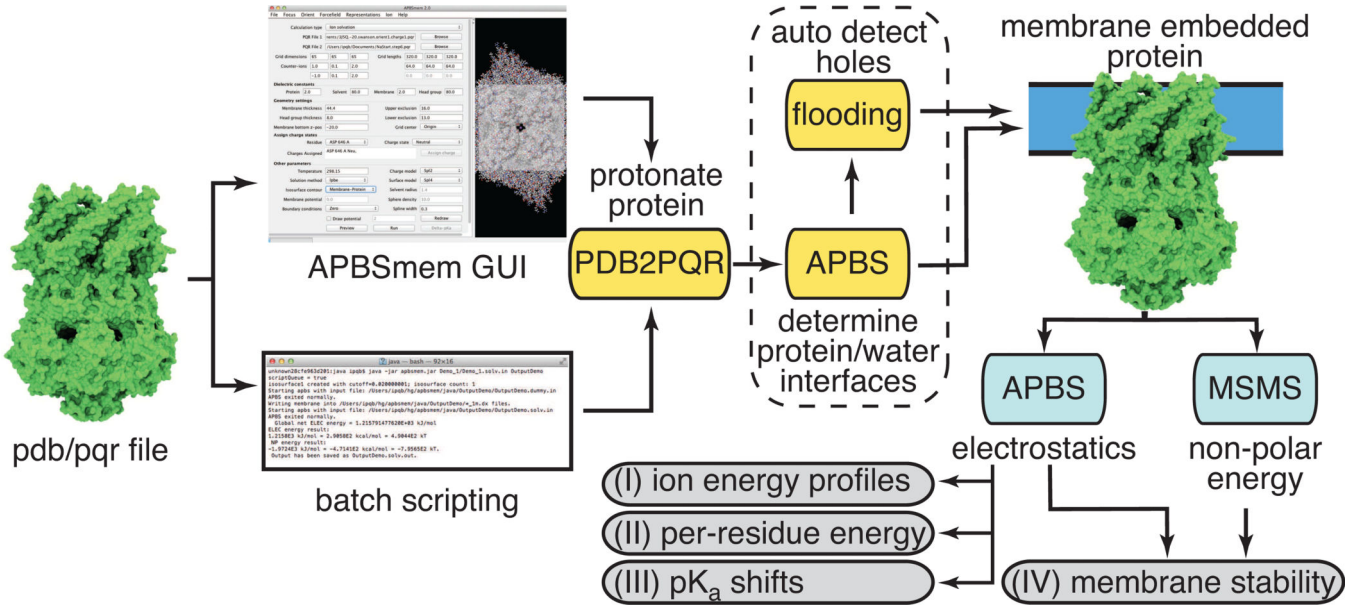

Figure 1. Workflow for APBSmem

PDB or PQR files (green) can be loaded into APBSmem through the GUI or via input files executed from a command line. The bundled PDB2PQR program will protonate PDB files followed by initial protein surface determination with APBS. A membrane flooding algorithm (see **Figure 2**) will add the presence of a low-dielectric membrane. APBS and MSMS can then be used to determine the energies for a number of situations outlined in Cases I-V.

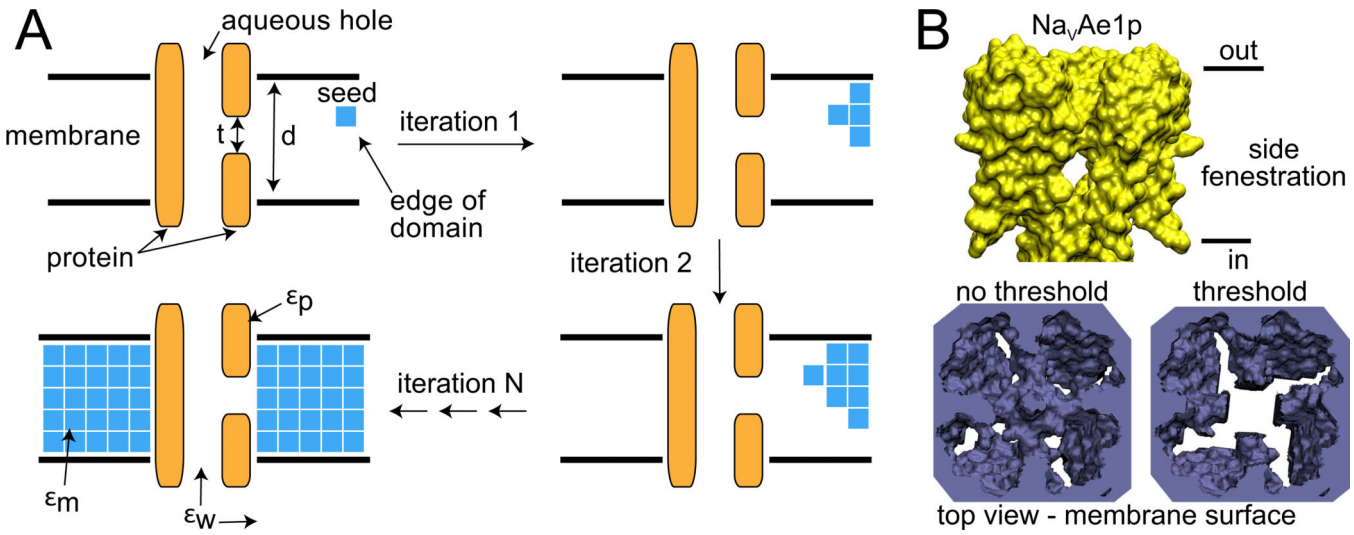

Figure 2. Automatic detection of aqueous channels

A, Membrane flooding method. Protein is orange, solution white, initial membrane boundaries black lines, and membrane blue. The membrane is added iteratively in small units starting from an initial seed at the outer boundary of the system. Membrane will not flood protein fenestrations with a vertical dimension less than t. **B,** Surface of the Na_VAe1p sodium channel showing large fenestrations in the hydrophobic core of the membrane (top). If no threshold is set of lipid penetration, Membrane fills the central aqueous cavity of the channel if no threshold is set (blue surface, bottom left); however, for t equal 8 Å, the membrane will not penetrate into aqueous cavities (bottom right).

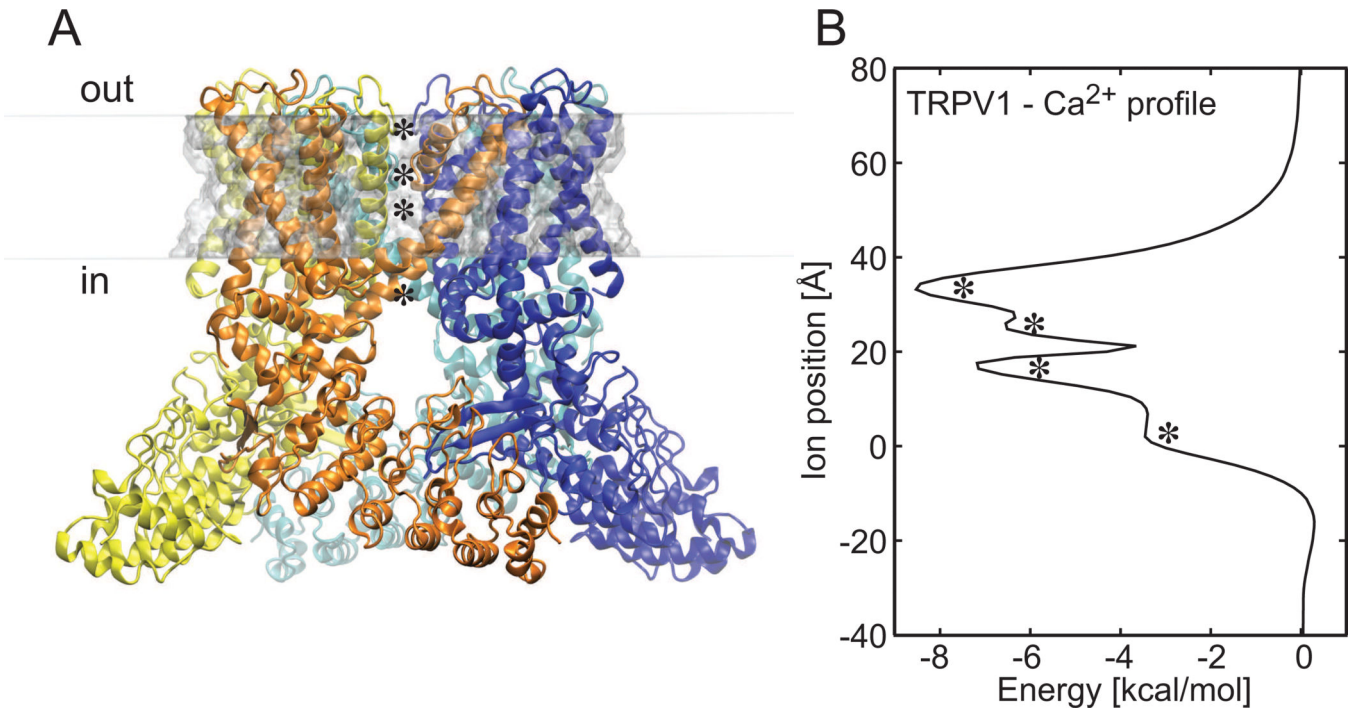

Figure 3. Ion stepping for potential energy profiles through TRPV1

A, Molecular image of the fully open TRPV1 tetramer bound to RTX and DkTx (PDB ID: 3j5q) colored by chain and embedded in a low-dielectric, ion-impermeable membrane. The upper and lower leaflets of the membrane are pale grey surfaces. Asterisks highlight positions along the channel that correspond to energy minima in B. **B,** Calcium ion solvation energy through TRPV1. The upper two minima are in the selectivity filter, the third from the top is in the cavity and the bottom position is near the inner gate.

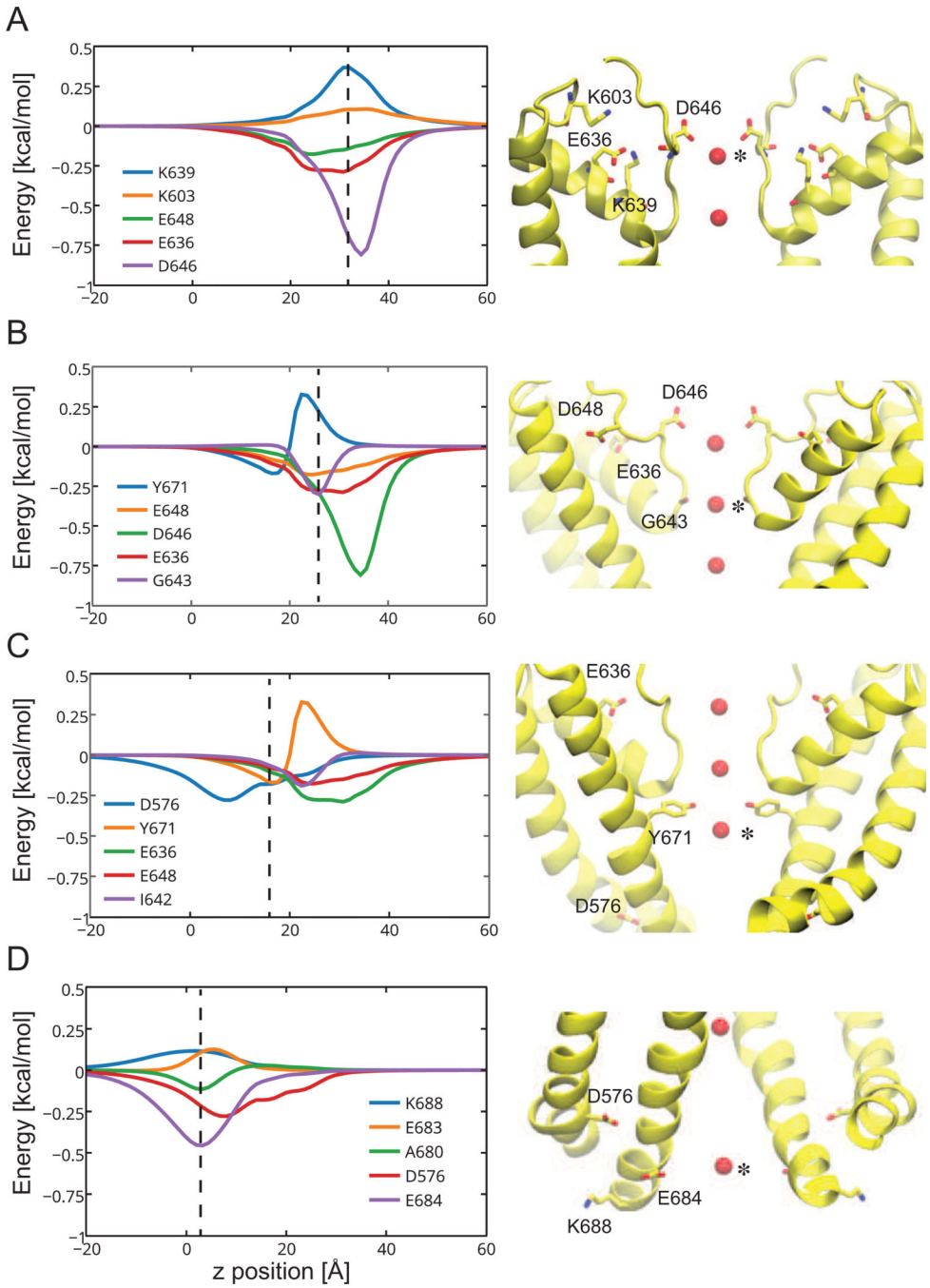

Figure 4. Critical residues contributing to the electrostatics of ion permeation through TRPV1

Top five residues interacting with the permeating ion (by absolute value) at each of the positions (A, 32 Å; B, 24.8 Å; C, 17.6 Å; and D, 2 Å) identified in **Figure 3**. The vertical dashed line is the ion position of interest at which the rank order was compiled, but interaction strengths are plotted through the entire channel. The molecular image to the right of each graph shows the ion (red asterisked sphere) at the z position corresponding to the dashed line. TRPV1 is yellow with impactful residues rendered in stick mode. For clarity, only two subunits of the channel are represented, and a Ca^{2+} ion is pictured at all four

positions for perspective, but calculations are performed with only a single ion in the channel.

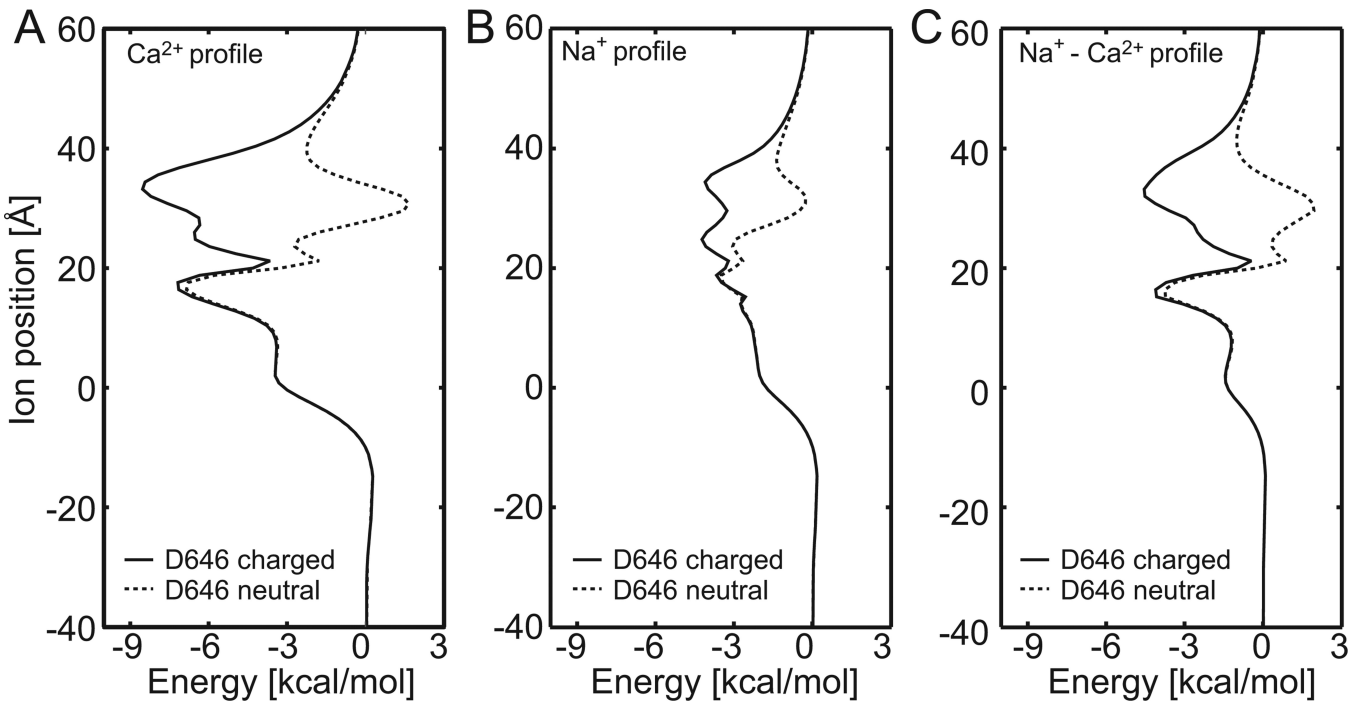

Figure 5. Selectivity is influenced by protonation state

A, B, Ion stepping profile with zero to four D646 residues neutralized for Ca^{2+} and Na^{+}, respectively. Note that the energies near 32 Å for both ions become comparable once all D646 residues are neutralized. **C,** Energy difference between profiles shown in panels A and B. This energy is the Ca^{2+} energy minus the Na^{+} energy.

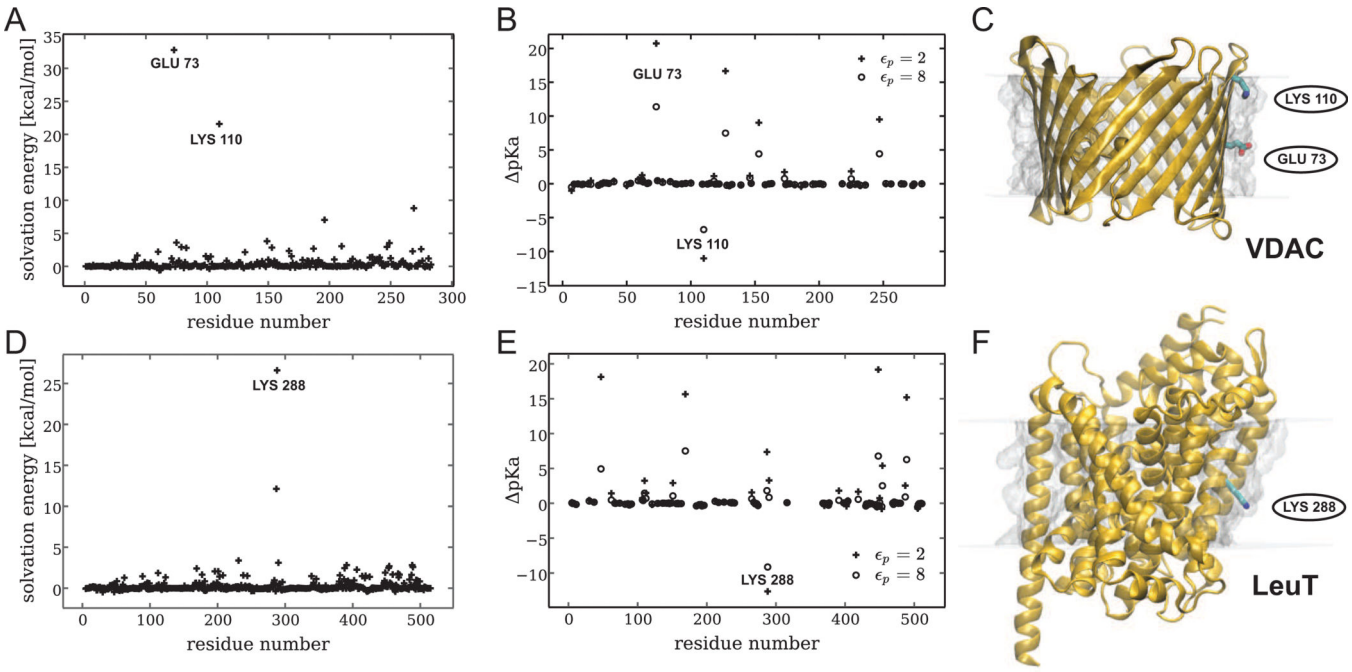

Figure 6. Membrane induced pK_a shifts

A, mVDAC1 (PDB ID: 3emn) per-residue solvation energy contributions. **B,** Membrane induced pK_a (ΔpK_a^2) shifts for mVDAC1 calculated with the protein dielectric set to 2 (+) or 8 (circle). **C,** Image of mVDAC1 showing E73 poking into the membrane and K110 in the headgroup. **D,** LeuT (PDB ID: 2a65) per-residue solvation energy contributions. **E,** Membrane induced pK_a shifts for LeuT with the protein dielectric set to 2 (+) or 8 (circle). **F,** LeuT showing K288 poking out into the membrane.

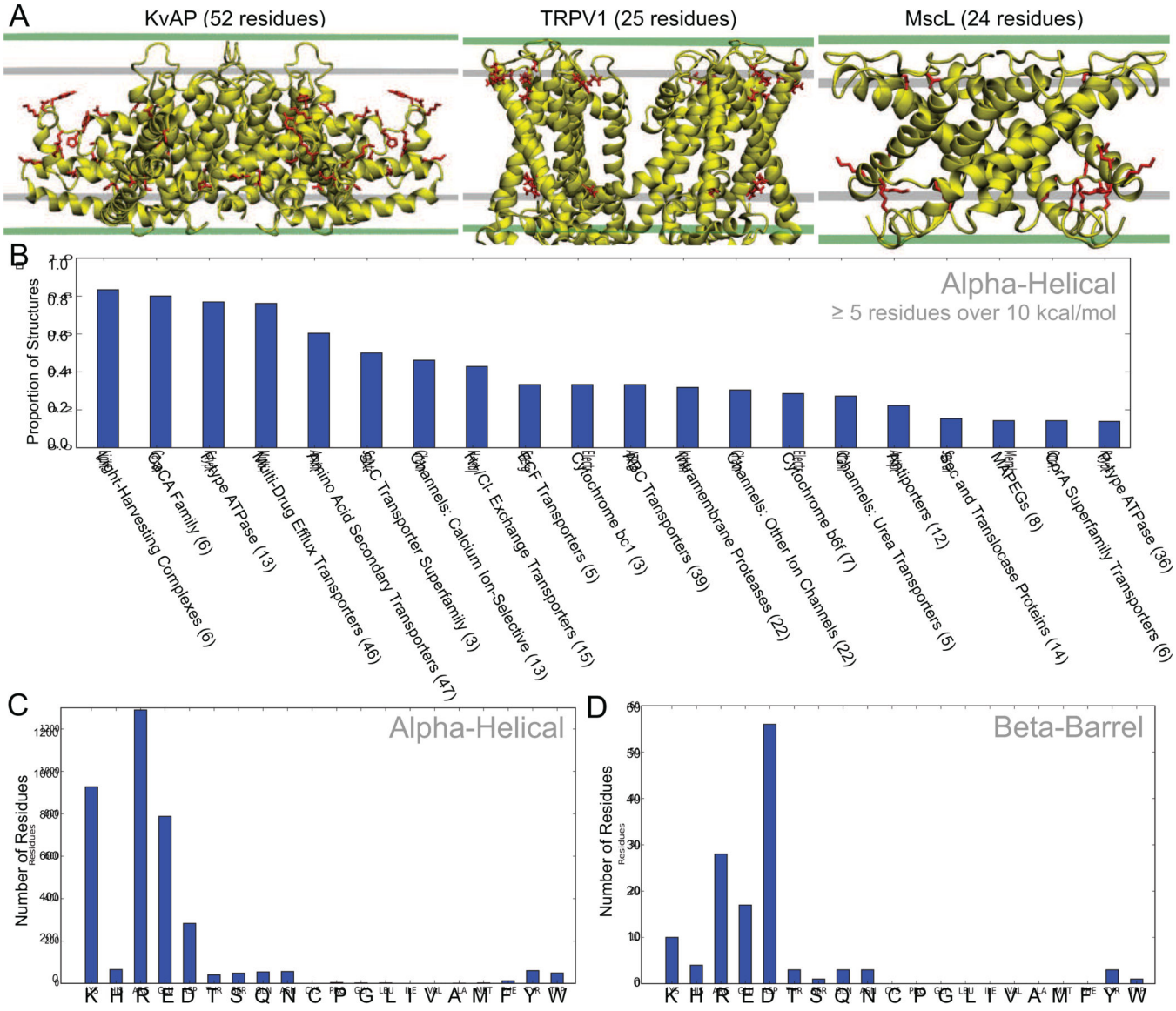

Figure 7. Electrostatic scan of multi-pass membrane proteins

A, Three of the structures with the largest number of electrostatically unfavorable residues: KvAP, TRPV1, and MscL (PBD IDs: 2a0l, 3j5r and 3hzq, respectively). Residues with over 10 kcal/mol electrostatic insertion penalty are shown in red licorice, and the total number of offending residues are given in parentheses. The water-head group and head group-tail interfaces are shown as green and white surfaces, respectively. **B,** Proportion of α-helical structures with five or more residues characterized as electrostatically unfavorable. Families are defined according to the Mpstruct database, and we excluded families with less than three structures used in the final calculations. The total number of structures analyzed for each family is given in parentheses. **C,D,** Total number of electrostatically unfavorable residues for α-helical and β-barrel proteins, respectively. In total, calculations involved 794 α-helical proteins and 215 β-barrel proteins.

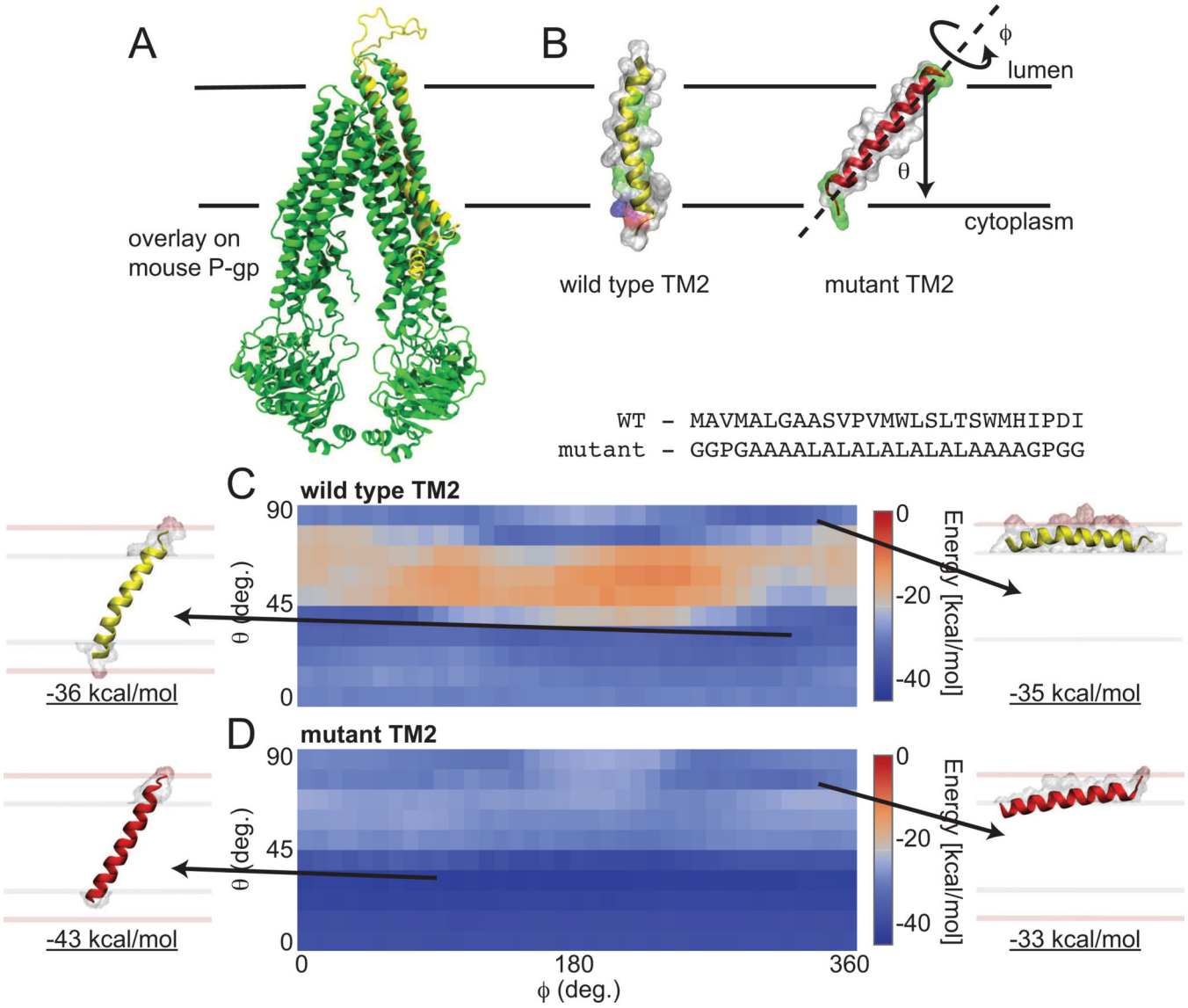

Figure 8. Membrane protein insertion energies

A, Superposition of homology model of Ste6p* 2TM construct (yellow) on the Pg-P template structure (green). **B,** Model of isolated TM2 from wild type (yellow on left) and poly-alanine/leucine construct (red on right) with molecular surface showing amino acid chemistry (white – hydrophobic, green – polar, blue – basic). Coordinate system corresponds to panels C and D. The primary sequence of each construct is shown at the bottom. **C-D,** Insertion energy heat map for wild type TM2 (**C**) and the artificial hydrophobic TM2 (**D**). The total energy consists of electrostatic and non-polar terms. The most stable configurations are fully inserted (θ less than 30°) or interfacial (θ near 90°). Minimum energy configurations of each o rientation are depicted to the left and right, respectively. The headgroup-water interface is pink and the headgroup-core interface is white.

Table 1

Input parameters.

molecule	TRPV1 (3j5q)	VDAC (3emn)	LeuT (2a65)	Ste6p*
force field	SWANSON	PARSE	PARSE	PARSE
counter ions	±1|e|, 0.1 M, 2.0 Å	±1|e|, 0.1 M, 2.0 Å	±1|e|, 0.1 M, 2.0 A	±1|e|, 0.1 M, 2.0 Å
temperature	298.15 K	298.15 K	298.15 K	298.15 K
grid dimensions	161×161×161	161×161×161	161×161×161	161×161×161
coarse grid size	320×320×320 $Å^3$	300×300×300 $Å^3$	300×300×300 $Å^3$	300×300×300 $Å^3$
medium grid size	160×160×160 $Å^3$	120×120×120 $Å^3$	120×120×120 $Å^3$	120×120×120 $Å^3$
fine grid size	64×64×64 $Å^3$	60×60×60 $Å^3$	60×60×80 $Å^3$	60×60×60 $Å^3$
protein dielectric	2	2 or 8	2 or 8	2
membrane dielectric	2	2.0	2.0	2.0
headgroup dielectric	80	80	80	80
solvent dielectric	80	80	80	80
membrane thickness	42.5 Å	39.9 Å	42.0 Å	39.9 Å
membrane bottom	−19.0 Å	−19.95 Å	−21.0 Å	−19.95 Å
headgroup thickness	8.0 Å	8.0 Å	9.0 Å	8.0 Å
upper/lower exclusion radii	16 Å/13 Å	18.5 Å/18.5 Å	12 Å/12 Å	12 Å/12 Å
grid center	origin	origin	origin	origin
solution method	npbe	npbe	npbe	npbe
boundary condition	zero	zero	zero	zero
membrane potential	0 mV	0 mV	0 mV	0 mV
charge model	spl2	spl2	spl2	spl2
surface model	spl4	mol	mol	mol
surface spline width	0.3 Å	N/A	N/A	N/A
solvent probe radius	N/A	1.4 Å	1.4 Å	1.4 Å
surface sphere density	N/A	10 $Å^{-2}$	10 $Å^{-2}$	10 $Å^{-2}$
ion initial position	(0 Å, 0 Å, −60 Å)	N/A	N/A	N/A
ion final position	(0 Å, 0 Å, 60 Å)	N/A	N/A	N/A
number of ion steps	100	N/A	N/A	N/A

Table 2

Predicted pK_a shifts for select charged groups.

protein	residue	calculation	method	pK_a
mVDAC1	Glu 73	pK_a^0 isolated amino acid in solution	experiment	4.50
		ΔpK_a^1 in protein in solution	PROPKA	0.31
		ΔpK_a^2 solution to membrane	Eq. 6	20.74
		modified pK_a	Eq. 8	25.55
mVDAC1	Lys 110	pK_a^0 isolated amino acid in solution	experiment	10.50
		ΔpK_a^1 in protein in solution	PROPKA	−0.26
		ΔpK_a^2 solution to membrane	Eq. 6	−11.03
		modified pK_a	Eq. 8	−0.79
LeuT	Lys 288	pK_a^0 isolated amino acid in solution	experiment	10.50
		ΔpK_a^1 in protein in solution	PROPKA	−0.20
		ΔpK_a^2 solution to membrane	Eq. 6	−12.64
		modified pK_a	Eq. 8	−2.34

Membrane dielectric is 2 for all calculations.